RSC Advances

PAPER

View Article Online
View Journal | View Issue

Cite this: *RSC Adv.*, 2023, **13**, 35429

Development and evaluation of polyacrylamide microspheres loaded with phloretin and tantalum for transcatheter arterial embolization

Liang Li, [a] Mao Qiang Wang, *[ab] Feng Duan, [b] Jin Long Zhang, [c] Bing Yuan, [b] Bao Cui, [d] Heng Zhang [ae] and Jie Yu Yan [b]

Received 28th August 2023
Accepted 21st November 2023

DOI: 10.1039/d3ra05841g

rsc.li/rsc-advances

Transcatheter arterial embolization is an effective treatment for liver cancer. However, the development of novel embolic agents remains a challenge. In this study, we evaluated polyacrylic acid microspheres loaded with phloretin and tantalum as potential embolic agents for liver cancer treatment. Microspheres were synthesised *via* emulsion polymerisation and characterised in terms of size, shape, and drug-loading efficiency. Nanosized tantalum powder (0 to 15%) was added to the microspheres as an X-ray blocking agent. The maximum drug-loading capacity of the microspheres was approximately 20 mg g^{-1}. The phloretin-loaded microspheres showed a sustained drug release profile *in vitro*. The microspheres were also evaluated for their *in vivo* anticancer efficacy in a rabbit VX2 liver tumour model. In conclusion, polyacrylic acid microspheres loaded with phloretin and tantalum have great potential as novel embolic agents for transcatheter arterial embolization for liver cancer treatment.

Introduction

Transcatheter arterial embolization (TAE) is an effective treatment for liver cancer. TAE can selectively embolize the main blood vessels of the tumour *via* arterial injection of embolic agents to cut off the nutritional supply to the tumour, thereby inhibiting tumour growth.[1] Currently, this method is widely used for the clinical treatment of liver cancer and other solid tumours. The blood supply to liver tumours is mainly delivered *via* the hepatic artery, whereas that of normal liver parenchyma is mainly provided by the hepatic portal vein; therefore, embolizing tumour blood supply vessels does not damage healthy liver parenchyma.[2] However, recanalisation of blood vessels after embolization or establishment of collateral circulation in the tumour restores nutritional supply to the tumour and leads to treatment failure. Therefore, tumour embolization is often combined with chemotherapy to enhance the antitumour effects of chemotherapeutic drugs. This approach is known as transarterial chemoembolization (TACE).[3]

Iodised oil is the most commonly used embolic agent in conventional TACE.[4–7] It is premixed with an aqueous solution of chemotherapeutic drugs and injected into tumour blood vessels through microcatheters for embolization.[6] However, it is insoluble in water and can only form a coarse emulsion with the chemotherapeutic solution. Therefore, chemotherapeutic drugs spread rapidly and do not remain in the tumour site for a long time.[5] In addition, systemic exposure to the chemotherapeutic drug can lead to serious adverse reactions similar to those of conventional chemotherapy, such as nausea and vomiting.[8,9] Therefore, the novel TACE strategy for liver cancer involves the use of drug-eluting microspheres to embolize the vessels supplying blood to the tumour.[10–12] Antitumour drugs, such as doxorubicin, carried by microspheres can be released slowly at the embolic site, prolonging the action time of chemotherapeutic drugs by approximately 1–3 months and reducing the distribution of the drugs throughout the body, thereby reducing the adverse reactions caused by these agents. However, at present, most commercial drug-eluting microspheres are not visible under X-ray irradiation; thus, the embolic condition after embolization cannot be evaluated by non-invasive examination.[12] Consequently, there remains a need to improve the application of drug-eluting microspheres in chemoembolization.

Currently, there has been an attempt to incorporate several contrast agents into microspheres for X-ray visualisation purposes, including bismuth sulfide, barium salts, and tantalum.[13–16] Among the aforementioned, tantalum nanoparticles are recognised as a promising X-ray contrast agent with excellent X-ray blocking effect and chemical stability. Moreover, they possess good biocompatibility and do not cause

[a]*Chinese PLA Medical School, Beijing 100853, PR China*
[b]*Department of Interventional Radiology, Chinese PLA General Hospital, Beijing 100853, PR China. E-mail: wangmq0117@163.com*
[c]*Department of Radiology, Beijing Tongren Hospital, Capital Medical University, Beijing 100730, PR China*
[d]*Department of Interventional, Bethune International Peace Hospital, Shijiazhuang, 050082, PR China*
[e]*Department of Radiology, National Clinical Research Center for Geriatric Diseases/Second Medical Center of Chinese PLA General Hospital, Beijing 100853, China*

significant adverse reactions, making them highly suitable as contrast agents for microsphere preparations.[13]

Phloretin (Ph), a new anticancer compound extracted from natural products, has been proven to have an inhibitory effect on various cancer cells including those of the liver, colon, and breast.[17–19] Ph selectively inhibits glucose transporter 2 to block glucose transport across the membrane of tumour cells, preventing their proliferation.[20] In this study, we aimed to prepare Ph-loaded porous polyacrylamide microspheres that can be detected under X-ray irradiation and examine its anti-tumour effects in animal models.

Results and discussion

Characterisation of phloretin emulsion

Table 1 presents the dynamic light scattering (DLS) results for the phloretin emulsion. The particle size, zeta potential, and drug content of the emulsion were analysed at 0 and 24 h. The mean size of the emulsion droplets was approximately 150 nm, with a polydispersity index (PDI) of 0.2, indicating homogeneous droplet size distribution. The zeta potential was approximately −20 mV, suggesting that the droplets were negatively charged. The average droplet size, zeta potential, and phloretin concentration of the emulsion exhibited no significant changes within 24 h when stored at 4 °C in the dark.

Characterisation of PMs

Fig. 1 shows the scanning electron microscopy (SEM) and X-ray images of the PMs and iodixanol (a commercially available X-ray contrast agent). When nanosized tantalum was added at a concentration of 0–10%, the shapes of the microspheres were intact, and a porous structure could be observed. No significant changes in the morphology of the PMs were observed, but some differences in the smaller pore sizes were noted under high magnification. After drug loading, the surface pores of the microspheres were filled with drug, but the smaller pores were not visible. The X-ray imaging revealed that adding nanosized tantalum powder at concentrations of 5–15% provided X-ray opacity to all PMs. At 5%, the contrast was slightly decreased, and the images were difficult to observe using digital subtraction angiography (DSA).

As the concentration increases, the contrast is significantly enhanced. Hence, at 10–15% concentrations, the DSA images should, theoretically, be very clear. As shown in Fig. 2, the particle sizes of PMs and Ph-PMs ranged from 150 μm to 300 μm, and the average particle size of Ph-PMs was slightly larger than that of PMs.

Table 1 DLS results of phloretin emulsion[a]

Time (h)	Size d (nm)	Zeta potential	PDI
0	144.33 ± 1.45	−19.77 ± 0.60	0.180 ± 0.020
24	144.73 ± 1.53	−19.57 ± 2.14	0.176 ± 0.016

[a] Data are shown as mean ± standard deviation, $n = 3$. DLS, dynamic light scattering; Ph, phloretin; PDI, polydispersity index.

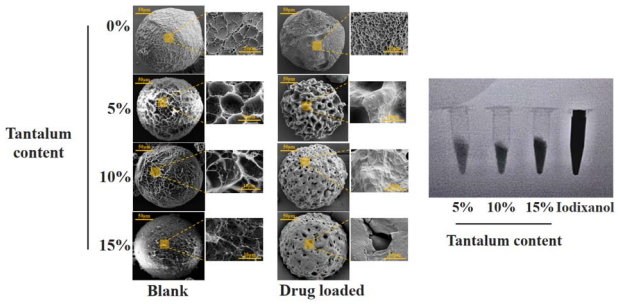

Fig. 1 SEM and X-ray images of PMs or Ph-PMs. SEM results showed that PMs possess a significant porous structure. Following drug loading, the pores were filled with the drug. DSA results show that the X-ray opacity of PMs increases with increasing concentrations of nanosized tantalum powder. DSA, digital subtraction angiography; PMs, polyacrylamide microspheres; Ph-PMs, phloretin-loaded polyacrylamide microspheres; SEM, scanning electron microscopy.

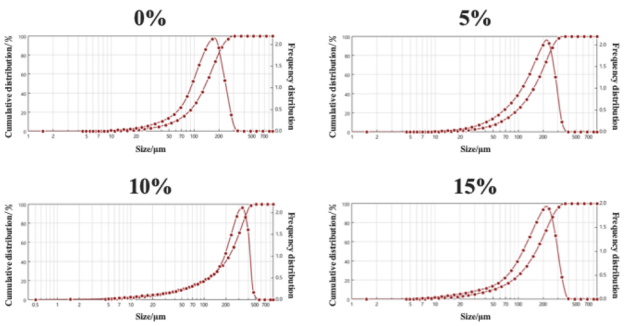

Fig. 2 Size distribution patterns of PMs with different tantalum content. PMs had a particle size ranging from 150–300 μm, and the addition of nanosized tantalum powder had no significant effect on the particle size of the microspheres. PMs, polyacrylamide microspheres.

Drug-loading capacity of PMs

PMs have a porous structure and good hydrophilicity; therefore, nanosized Ph droplets can be loaded by swelling. To this end, the dehydrated microspheres were completely immersed in Ph emulsion, and samples were taken at 15, 30, and 60 min to determine Ph content in the microspheres. As shown in Table 2, maximum drug loading (approximately 20 mg g^{-1}) was achieved at 30 min. None of the groups showed any significant differences in drug-loading capacity.

In vitro drug release

As shown in Fig. 3, the drug release behaviour of the Ph-PMs can be classified into two phases: burst release and sustained release. The period from 0–6 h can be described as the burst release stage, during which cumulative drug release attains approximately 20%. As a typical phenomenon observed in most microsphere formulations, this may be advantageous, as concentrations with tumour growth-inhibiting properties can be achieved by administering higher initial doses of therapeutic drug(s) during embolization. Following the burst release stage, the release rate of the residual drugs becomes relatively slow as

Table 2 pH-loading capacity of PMs[a]

	Drug loading mg g^{-1}		
Tantalum content/%	15 min	30 min	60 min
0	12.17 ± 1.39	17.37 ± 1.85	21.38 ± 4.23
5	14.5 ± 1.50	19.89 ± 4.00	21.3 ± 1.82
10	15.86 ± 0.82	22.14 ± 1.51	23.4 ± 2.06
15	14.84 ± 1.21	23.46 ± 1.41	24.15 ± 0.56

[a] Data are shown as mean ± standard deviation, $n = 3$. Ph, phloretin; PMs, polyacrylamide microspheres.

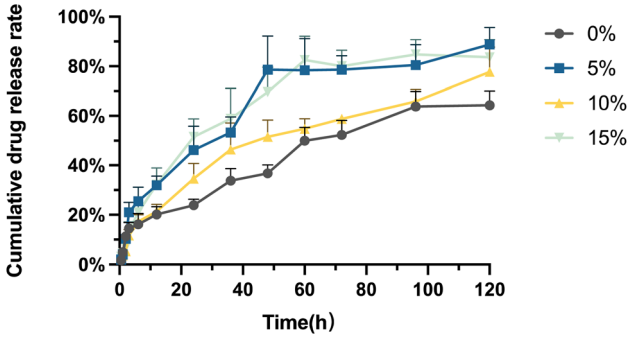

Fig. 3 Cumulative drug release of Ph-PMs with different tantalum concentrations (0, 5, 10, and 15%). Data are shown as mean ± standard deviation, $n = 3$. Ph-PMs, phloretin-loaded polyacrylamide microspheres.

they are usually located within the interior of the microspheres. Thus, the subsequent release phase could enable sustained drug release in the tumour area, prolonging the time of tumour growth inhibition. The results indicate that the cumulative drug release reached 70–90% on day 5.

In vitro cytotoxicity of phloretin emulsion and PMs

Fig. 4 shows the cytotoxicity of free phloretin, phloretin emulsion, and PMs. The phosphate buffered saline (PBS) extract of PMs was used to evaluate *in vitro* cytotoxicity, as the precipitation of PMs in the medium may cause cell damage. The results revealed that the antitumour effect of the phloretin emulsion was similar to that of phloretin *in vitro*, indicating that the antitumour effect of the drug was not weakened after emulsion preparation. Moreover, the extract containing PMs displayed no significant cytotoxicity, consistent with the results of PBS and blank emulsion, suggesting good safety and biocompatibility of blank PMs.

In vivo anticancer evaluation

The rabbit VX2 liver tumour model has been widely used in TACE studies. With the assistance of existing technologies, the main blood vessels of liver tumours can be observed using real-time X-ray equipment, and TACE can be performed *via* femoral artery catheterisation in the rabbit model. The antitumour effects of blank PMs and Ph-PMs were compared. Moreover, the liver function and white blood cell counts of the subjects were

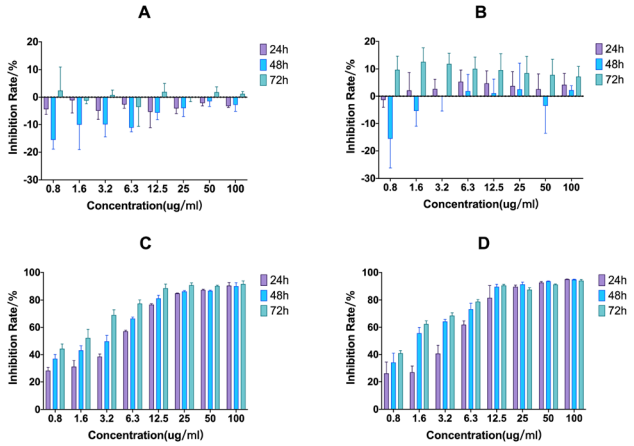

Fig. 4 *In vitro* cytotoxicity at 24–72 h. (A) Inhibition rate of the blank emulsion; (B) inhibition rate of the PMs leaching solution; (C) inhibition rate of free Ph; (D) inhibition rate of the phloretin emulsion. PMs, polyacrylamide microspheres; Ph, phloretin. Data are shown as mean ± standard deviation, $n = 6$.

monitored to assess the *in vivo* safety of both PMs and Ph-PMs. Computed tomography (CT) scan results on days 0 and 10 of TACE revealed that the PMs and Ph-PMs successfully embolised the blood vessels feeding the tumour tissue (Fig. 5). Both the PMs and Ph-PMs exhibited excellent contrast profiles under X-ray irradiation. The tumour volume results indicated that the control group infused with saline alone exhibited a significant increase in tumour volume. Conversely, embolization with PMs and Ph-PMs significantly inhibited tumour growth. Furthermore, the Ph-PMs group showed a slower tumour growth rate, indicating a superior therapeutic effect compared to blank PMs.

Blood tests showed no statistically significant differences in the total white blood cell counts of each group, indicating that no severe infection occurred in the animals after embolization (Fig. 6). In the PMs and Ph-PMs groups, aspartate transaminase and total bilirubin (TBIL) levels significantly increased on day 1, decreased significantly on day 3, and returned to baseline levels on day 7, suggesting that microsphere embolization could cause a certain degree of hepatic injury that can recover in a short period, with minor effects on normal liver function.

Histological analysis of tumour tissue

Tumour tissue were sampled and subjected to haematoxylin and eosin (HE) staining and terminal deoxynucleotidyl transferase dUTP nick end labelling (TUNEL) assays on day 10 (Fig. 7). In the saline group, HE staining revealed good tumour tissue activity and prominent general characteristics of tumour tissue, such as noticeable nuclear enlargement. The necrotic areas of the tumours in the PMs and Ph-PMs groups were clearly visible, demonstrating that embolization can effectively suppress tumour tissue activity. In the TUNEL assay, the apoptotic areas in the tumours in the PMs and Ph-PMs groups were markedly larger than that in the saline group. Furthermore, the level of apoptosis in tumour cells was more significant in the Ph-PMs group than in the PMs group. These results

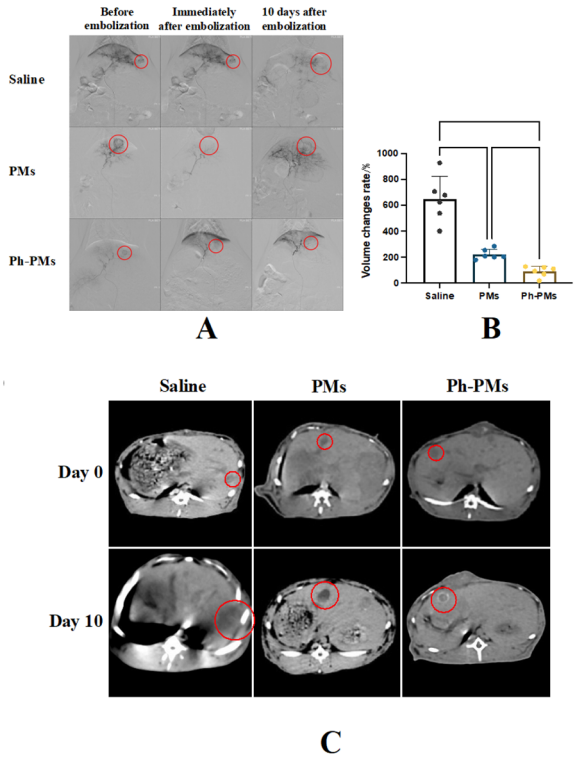

Fig. 5 *In vivo* anticancer evaluation results. (A) DSA images during different stages of the experiment. Before embolization; immediately after embolization (day 0); and 10 days after embolization. (B) Tumour volume change rates. (C) CT scan images showing the changes in the tumours on day 0 (before embolization) and 10 days after embolization. Red circles indicate the tumour locations in the image. DSA, digital subtraction angiography; PMs, polyacrylamide microspheres; Ph-PMs, phloretin-loaded polyacrylamide microspheres.

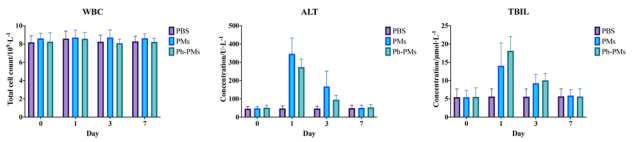

Fig. 6 Blood test results. WBC, white blood cell count; ALT, alanine aminotransferase; TBIL, total bilirubin. Data are shown as mean ± standard deviation, $n = 6$. *$p < 0.05$, **$p < 0.01$, ***$p < 0.001$.

showed the enhanced *in vivo* antitumour efficacy of Ph-PMs, which was achieved by combining phloretin and mechanical embolization.

Experimental

Materials

Egg phosphatidylcholine (EPC) was purchased from Lipoid GmbH (Ludwigshafen, Germany). Poly(vinyl alcohol) 1788 (PVA-1788), paraffin liquid, Span-80, and phloretin were purchased from Energy Chemical (Shanghai, China). *N*,*N*,*N*′,*N*′-Tetramethylethylenediamine (TEMED) was purchased from Shanghai Aladdin Biochemical Technology Co., Ltd. Acrylic acid, *N*,*N*′-methylenebis(2-propenamide), and ammonium persulfate were

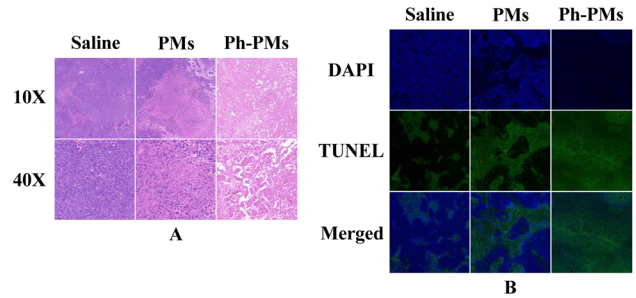

Fig. 7 Tumour pathological section results. (A) HE staining results; (B) TUNEL staining results. DAPI (blue colour) indicates the cell nucleus; TUNEL (green colour) indicates apoptotic cells. PMs, polyacrylamide microspheres; Ph-PMs, phloretin-loaded polyacrylamide microspheres. DAPI, 4′,6-diamidino-2-phenylindole; TUNEL, terminal deoxynucleotidyl transferase dUTP nick end labelling; PBS, phosphate buffered saline; HE, haematoxylin and eosin.

purchased from Shanghai Macklin Biochemical Co., Ltd. Foetal bovine serum, Dulbecco's modified Eagle's medium (DMEM)/high glucose, and penicillin–streptomycin solution were purchased from Yeasen Biotechnology (Shanghai) Co., Ltd. Nanosized tantalum powder was purchased from Shanghai Macklin Biochemical Technology Co., Ltd.

Animals. Twenty-four New Zealand white rabbits (provided by the Animal Experiment Center of the Chinese PLA General Hospital) of either sex weighing 2.0–2.5 kg were used. All rabbits were housed individually in professional animal facilities under standard conditions and provided with standard rabbit food and purified water. The environmental conditions were maintained at a temperature of 18–22 °C, a humidity of 55 ± 6%, and a 12 h light–dark cycle. All animal procedures were performed in accordance with the Guidelines for Care and Use of Animal Experiment Center of Chinese PLA General Hospital and approved by the Animal Ethics Committee of Chinese PLA General Hospital.

Methods

Preparation and characterisation of phloretin emulsion. Phloretin emulsions were prepared using the high-pressure homogenisation method. Briefly, 50 mg phloretin was dissolved with 0.2 g of ethanol and mixed with 1.5 g medium chain triglyceride (MCT). Then, 46.25 g of deionised water and phloretin–MCT solution were added to 2.0 g of EPC, and a high-speed disperser (T25, IKA, Germany) was used to form a suspension. The suspension was dispersed using a high-pressure homogeniser (MS1001L PANDA, Niro Soavi, Italy): the first valve pressure was 1000 bar, the second valve pressure was 100 bar, the homogenisation time was 5 min, and the homogenisation temperature was 4 °C. Size distribution and zeta potential of the resultant emulsion were determined using DLS. Phloretin content in the emulsion was determined by high-performance liquid chromatography (HPLC) using a C18 column (50 mm × 2 mm, 3 μm). The eluent was a mixture of water and acetonitrile (25 : 75, v/v). The detection wavelength was set at 280 nm. All samples were stored at 4 °C in the dark.

Preparation of PMs. PMs were prepared using the inverse suspension polymerisation method. Liquid paraffin containing 0.5% Span 80 was used as the oil phase. The oil phase was subjected to 500 rpm magnetic stirring and preheated to 55 °C. The aqueous phase consisted of 0.5 g methylene bisacrylamide, 2.2 g ammonium persulfate, 5 g acrylic acid, 0.5 g polyvinyl alcohol, and 6.5 g water. Nanosized tantalum powder (5%, 10%, and 15%) was added as a contrast agent in the aqueous phase. Under nitrogen protection, the aqueous phase was added to the preheated oil phase and stirred for 10 min to form a suspension. Then, 500 μL TEMED was added into the suspension to trigger polymerisation. After further stirring for 30 min, microspheres with particle sizes of 100–300 μm were collected and washed with *n*-heptane. Freeze-drying was performed to remove water from the PMs.

Size distribution, morphology, and X-ray visibility. PMs containing varying concentrations of nanosized tantalum were prepared using previously described procedures. The particle size distribution of the PMs was determined using a laser particle size analyser (MS2000, Malvern, England) and SEM (GeminiSEM 300, ZEISS, Germany) was performed to assess the morphology of the microspheres. Before imaging, the PMs were coated with gold. Real-time X-ray imaging was also conducted to evaluate the X-ray visibility of the PMs.

Drug-loading capacity of PMs. To identify the maximum drug-loading capacity of the PMs, dry PMs were mixed and stirred in the phloretin emulsion. Phloretin emulsion was loaded into porous PMs by swelling. At a predetermined time, the PMs were separated by centrifugation, washed thrice with deionised water, and freeze-dried to remove water. The PMs were then soaked in methanol and vortexed for 15 min to incorporate the phloretin into the PMs. HPLC was used to determine the drug content in the supernatant after centrifugation.

***In vitro* drug release.** To evaluate the *in vitro* drug release profile of Ph-PMs, PBS solutions at a of pH 7.4 were used. Specifically, 0.1 g of Ph-PMs was immersed in 50 mL of release medium and agitated at a speed of 100 rpm, with the temperature maintained at 37 ± 0.5 °C. At predetermined intervals, 0.5 mL samples were withdrawn, and an equivalent volume of fresh medium was promptly replenished. The concentration of phloretin in the medium was determined using HPLC. All assays were performed in triplicate in the dark. Cumulative drug release from the Ph-PMs was calculated as follows:

$$\text{Cumulative drug release} = \frac{V_0 \times C_t + V_s \times \sum_{1}^{n-1} C_n}{m} \times 100\%$$

where m is the total mass of the drug in the Ph-PMs, V_0 is the initial volume of the release medium, V_s is the sampling volume, C_t is the final drug concentration, and C_n is the drug concentration determined before C_t.

***In vitro* cytotoxicity of phloretin emulsion and PMs.** *In vitro* cytotoxicity was evaluated using HepG2 cell lines. Briefly, HepG2 cells were seeded in 96-well plates at a density of 8×10^3 cells per well and allowed to adhere for 24 h. The culture medium in each well was then replaced with free phloretin, phloretin emulsion, PMs leaching solution, or blank emulsion diluted with fresh complete DMEM. Cell inhibition rate was determined at 24, 48, and 72 h using the CCK8 method and calculated as follows:

$$\text{Inhibition rate} = 100\% - \frac{OD_{test} - OD_{blank}}{OD_{control} - OD_{blank}} \times 100\%$$

where OD_{blank} is the optical density of the blank well (PBS and CCK8 reagent), OD_{test} is the optical density of the test group, and $OD_{control}$ is the optical density of the control group. The detection wavelength was 450 nm.

***In vivo* anticancer evaluation.** Twenty-four New Zealand white rabbits weighing 2.0–2.5 kg were used to evaluate the therapeutic efficacy of Ph-PMs. Bioactive VX2 tumour tissue was aseptically cut into 1–2 mm^3 pieces and transplanted into the liver of rabbits. Following the procedure, all animals were continuously intramuscularly injected with penicillin sodium for three consecutive days to prevent infection. When the tumour size reached 50–100 mm^3, the rabbits were randomised into three groups: blank ($n = 8$), PMs ($n = 8$), and Ph-PMs ($n = 8$). CT-guided microcatheters were used to infuse the main blood vessels of the tumour. Animals in the blank group were infused with 0.5 mL saline; the PMs group was injected with no more than 0.5 g of PMs suspended in saline; the Ph-PMs group was injected with no more than 0.5 g of Ph-PMs microspheres pre-dispersed in saline.

On days 0 and 10 following TACE, all animals were performed abdominal CT scans. The largest (L) and smallest (S) tumour diameters were recorded, and the tumour volumes and tumour volume change rates were subsequently estimated as follows:

$$\text{Tumor volume} = \frac{L \times S^2}{2}$$

$$\text{Tumor volume change rate} = \frac{\text{tumor volume (day 10)}}{\text{tumor volume (day 0)}} \times 100\%$$

White blood cells and liver function test. At 0, 1, 3, and 7 days after TACE, blood samples were collected from the animals in each group. Total white blood cells were counted, and glutamic pyruvic transaminase and TBIL levels were measured using ELISA kits.

Histological analysis of tumour tissue. On day 10 following TACE, all the animals were euthanised. Tumour tissues were harvested immediately and fixed in 4% paraformaldehyde. HE staining and terminal deoxynucleotidyl TUNEL staining were performed to observe histopathological alterations and cell apoptosis.

Conclusions

In this study, X-ray-visible microspheres carrying phloretin were prepared and evaluated both *in vitro* and *in vivo*. The Ph-PMs group demonstrated a significant improvement in the anti-tumour effect compared to the PMs group, indicating the

potential utility of Ph-PMs in TACE for liver cancer treatment. Further studies are required to determine the long-term safety and synergistic anticancer effects of other chemotherapeutic drugs carried by PMs. Our findings provide a promising concept for microsphere-based interventions in liver cancer treatment.

Author contributions

Liang Li, Maoqiang Wang contributed to the conception of the study; Liang Li, Jin Long Zhang, Bing Yuan, Bao Cui performed the experiment; Feng Duan, Jie Yu Yan contributed significantly to the analysis and manuscript preparation; Liang Li, Heng Zhang performed the data analyses and wrote the manuscript.

Conflicts of interest

There are no conflicts to declare.

Acknowledgements

This study was supported by National Natural Science Foundation of China Grant 82072023.

References

1 M. Zuo and J. Huang, The history of interventional therapy for liver cancer in China, *J. Interv. Med.*, 2018, **1**(2), 70–76.
2 J. L. Raoul, A. Forner, L. Bolondi, T. T. Cheung, R. Kloeckner and T. de Baere, Updated use of TACE for hepatocellular carcinoma treatment: how and when to use it based on clinical evidence, *Cancer Treat. Rev.*, 2019, **72**, 28–36.
3 S. B. Yang, J. H. Zhang, Y. F. Fu and R. Wang, TACE with portal vein radioactive seeds for HCC with portal vein tumor thrombus: a meta-analysis, minimally invasive therapy & allied technologies, *Minim Invasive Ther. Allied Technol.*, 2022, **31**(6), 856–864.
4 J. H. Kim, P. N. Kim, H. J. Won and Y. M. Shin, Viable hepatocellular carcinoma around retained iodized oil after transarterial chemoembolization: radiofrequency ablation of viable tumor plus retained iodized oil versus viable tumor alone, *AJR, Am. J. Roentgenol.*, 2014, **203**(5), 1127–1131.
5 M. Tsurusaki and T. Murakami, Surgical and Locoregional Therapy of HCC: TACE, *Liver Cancer*, 2015, **4**(3), 165–175.
6 T. Ueda, S. Murata, D. Yasui, T. Mine and S. Kumita, Comparison of the antitumor efficacy of transcatheter arterial chemoembolization with a miriplatin-iodized oil suspension and a cisplatin-iodized oil suspension for hepatocellular carcinoma, *Hepatol. Res.*, 2013, **43**(10), 1071–1077.
7 K. Yoshimitsu, Transarterial chemoembolization using iodized oil for unresectable hepatocellular carcinoma: perspective from multistep hepatocarcinogenesis, *Hepatic Med.*, 2014, **6**, 89–94.
8 I. M. Zraik and Y. Heß-Busch, Management of chemotherapy side effects and their long-term sequelae, *Urologe A*, 2021, **60**(7), 862–871.
9 C. E. Knezevic and W. Clarke, Cancer Chemotherapy: The Case for Therapeutic Drug Monitoring, *Ther. Drug Monit.*, 2020, **42**(1), 6–19.
10 Q. Shi, J. Liu, T. Li, C. Zhou, Y. Wang, S. Huang, C. Yang, Y. Chen and B. Xiong, Comparison of DEB-TACE and cTACE for the initial treatment of unresectable hepatocellular carcinoma beyond up-to-seven criteria: a single-center propensity score matching analysis, *Clin. Res. Hepatol. Gastroenterol.*, 2022, **46**(5), 101893.
11 A. Ghosh, V. Gupta, A. Al Khalifah and N. M. Akhter, Transradial versus transfemoral arterial access in DEB-TACE for hepatocellular carcinoma, *J. Clin. Imaging Sci.*, 2022, **12**, 38.
12 F. Melchiorre, F. Patella, L. Pescatori, F. Pesapane, E. Fumarola, P. Biondetti, P. Brambillasca, C. Monaco, A. M. Ierardi, G. Franceschelli and G. Carrafiello, DEB-TACE: a standard review, *Future Oncol.*, 2018, **14**(28), 2969–2984.
13 J. Zeng, L. Li, H. Zhang, J. Li, L. Liu, G. Zhou, Q. Du, C. Zheng and X. Yang, Radiopaque and uniform alginate microspheres loaded with tantalum nanoparticles for real-time imaging during transcatheter arterial embolization, *Theranostics*, 2018, **8**(17), 4591–4600.
14 Y. Shen, B. Zhang, Z. Yi, L. Zhang, J. Ling, S. Wang, Z. Sun, M. Z. Iqbal and X. Kong, Microfluidic fabrication of X-ray-visible sodium hyaluronate microspheres for embolization, *RSC Adv.*, 2023, **13**(30), 20512–20519.
15 Q. Wang, K. Qian, S. Liu, Y. Yang, B. Liang, C. Zheng, X. Yang, H. Xu and A. Q. Shen, X-ray visible and uniform alginate microspheres loaded with in situ synthesized BaSO4 nanoparticles for in vivo transcatheter arterial embolization, *Biomacromolecules*, 2015, **16**(4), 1240–1246.
16 M. Horikawa, M. Ishikawa, B. T. Uchida, J. A. Kaufman and K. Farsad, Practical Tantalum Coating of Microspheres for Experimental Visualization under Fluoroscopy and CT, *J. Vasc. Intervent. Radiol.*, 2016, **27**(1), 127–132.
17 A. F. Abdel-Wahab, W. Mahmoud and R. M. Al-Harizy, Targeting glucose metabolism to suppress cancer progression: prospective of anti-glycolytic cancer therapy, *Pharmacol. Res.*, 2019, **150**, 104511.
18 J. L. Kim, D. H. Lee, C. H. Pan, S. J. Park, S. C. Oh and S. Y. Lee, Role of phloretin as a sensitizer to TRAIL-induced apoptosis in colon cancer, *Oncol. Lett.*, 2022, **24**(3), 321.
19 S. Saraswati, A. Alhaider, A. M. Abdelgadir, P. Tanwer and H. M. Korashy, Phloretin attenuates STAT-3 activity and overcomes sorafenib resistance targeting SHP-1-mediated inhibition of STAT3 and Akt/VEGFR2 pathway in hepatocellular carcinoma, *Cell Commun. Signaling*, 2019, **17**(1), 127.
20 B. Y. Choi, Biochemical Basis of Anti-Cancer-Effects of Phloretin-A Natural Dihydrochalcone, *Molecules*, 2019, **24**(2), 278.